Theses and Dissertations   1. Thesis and Dissertation Collection, all items

1990

Attitude control of flexible structures

Ward, Christina C.

http://hdl.handle.net/10945/37569

NAVAL POSTGRADUATE SCHOOL
Monterey, California

AD-A240 520

DTIC
ELECTE
SEP 13 1991
S D
D

THESIS

ATTITUDE CONTROL OF
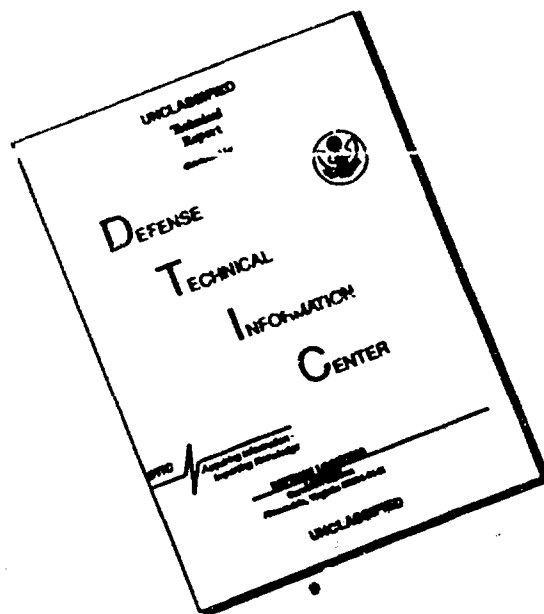FLEXIBLE STRUCTURES

by

Christina C. Ward

September 1990

Thesis Advisor: Prof. Brij N. Agrawal

91

91-10462

DISCLAIMER NOTICE

Unclassified

SECURITY CLASSIFICATION OF THIS PAGE

REPORT DOCUMENTATION PAGE					Form Approved OMB No 0704-0188
1a REPORT SECURITY CLASSIFICATION Unclassified			1b RESTRICTIVE MARKINGS None		
2a SECURITY CLASSIFICATION AUTHORITY Unclassified			3 DISTRIBUTION AVAILABILITY OF REPORT Approved for public release. Distribution unlimited.		
2b DECLASSIFICATION DOWNGRADING SCHEDULE					
4 PERFORMING ORGANIZATION REPORT NUMBER(S) Naval Postgraduate School			5 MONITORING ORGANIZATION REPORT NUMBER(S) Naval Postgraduate School		
6a NAME OF PERFORMING ORGANIZATION Naval Postgraduate School		6b OFFICE SYMBOL (If applicable)	7a NAME OF MONITORING ORGANIZATION Naval Postgraduate School		
6c ADDRESS (City, State and ZIP Code) Monterey, CA 93943-5000			7b ADDRESS (City, State and ZIP Code) Monterey, CA 93943-5000		
8a NAME OF FUNDING SPONSORING ORGANIZATION		8b OFFICE SYMBOL (If applicable)	9 PROCUREMENT INSTRUMENT IDENTIFICATION NUMBER		
8c ADDRESS (City, State and ZIP Code)			10 SOURCE OF FUNDING NUMBERS		

PROGRAM ELEMENT NO	PROJECT NO	TASK NO	WORK UNIT ACCESSION NO

11 TITLE (Include Security Classification)

ATTITUDE CONTROL OF FLEXIBLE STRUCTURES

12 PERSONAL AUTHORS

WARD, Christina C.

13a TYPE OF REPORT Master's Thesis	13b TIME COVERED FROM ____ TO ____	14 DATE OF REPORT (Year, Month Day) September 1990	15 PAGE COUNT 60

16 SUPPLEMENTARY NOTATION

The views expressed in this thesis are those of the author and do not reflect the official policy or position of the Department of Defense or US Govt.

17	COSATI CODES		18 SUBJECT TERMS (Continue on reverse if necessary and identify by block number)
FIELD	GROUP	SUB-GROUP	Attitude control, Flexible structures

19 ABSTRACT Continue on reverse if necessary and identify by block number)

The experimental set-up for laboratory study of spacecraft control/structural interaction have been designed. Design specifications have been derived, and all the actuators and sensors have been selected except the end-point displacement sensing of the arm. The mainbody and the flexible arm have been fabricated to meet design criteria. The equations of motion for the experimental model have been derived and natural frequencies determined. The natural frequencies of the flexible arm has been determined experimentally and compared with analytical predictions obtained by using the GIFTS finite element analysis program. The experimental and analytical results are in good agreement except the first mode.

20 DISTRIBUTION AVAILABILITY OF ABSTRACT ☒ UNCLASSIFIED UNLIMITED ☐ SAME AS RPT ☐ DTIC USERS	21 ABSTRACT SECURITY CLASSIFICATION Unclassified
22a NAME OF RESPONSIBLE INDIVIDUAL Dr. Brij Agrawal	22b TELEPHONE (Include Area Code) 408-646-3888	22c OFFICE SYMBOL AA/Ag

DD Form 1473, JUN 86   Previous editions are obsolete   SECURITY CLASSIFICATION OF THIS PAGE

S/N 0102-LF-014-6603   Unclassified

i

Attitude Control of
Flexible Structures

by

Christina C. Ward
Lieutenant, United States Navy
B.A., Nasson College, 1978

Submitted in partial fulfillment of the
requirements for the degree of

MASTER OF SCIENCE IN ASTRONAUTICAL ENGINEERING

from the

NAVAL POSTGRADUATE SCHOOL
September 1990

Author: _____
Christina C. Ward

Approved By: _____
Brij N. Agrawal, Thesis Advisor

_____
Harold Titus, Second Reader

_____
E. Roberts Wood, Chairman, Department of
Aeronautical and Astronautical Engineering

ii

ABSTRACT

The experimental set-up for laboratory study of spacecraft control/structural interaction has been designed. Design specifications have been derived, and all the actuators and sensors have been selected except the end-point displacement sensing of the arm. The mainbody and the flexible arm have been fabricated to meet design criteria.

The equations of motion for the experimental model have been derived and natural frequencies determined. The natural frequencies of the flexible arm have been determined experimentally and compared with analytical predictions obtained by using the GIFTS finite element analysis program. The experimental and analytical results are in good agreement except the first mode.

iii

TABLE OF CONTENTS

I. INTRODUCTION

A. THE CONTROL OF FLEXIBLE STRUCTURES

Flexible structures have become an integral part of modern spacecraft design for a variety of reasons. Deployable structures extending several meters into space used for solar arrays are required for todays high powered satellites. Radar reflectors of large diameter are used for communication satellites. Meanwhile, as the systems expand in size, weight constraints continue to plague the satellite designer. Hence, lighter and flexible structures are often used. This results in lower structural natural frequencies.

The large antenna reflectors require higher attitude pointing accuracy. In order to provide higher attitude pointing accuracy, the control bandwidth has to be increased. Because of the decrease in the structural natural frequencies and increase in control bandwidth, there is a high possibility of the structural frequency falling into the control bandwidth, resulting in control/structure interaction.

For some space applications, the flexible structure will require active control. As a result, current and future spacecraft study of control/structure interaction has become a challenging problem.

1

B. BACKGROUND.

The control of rigid body dynamic systems has been a subject of study for many years. Controlling three-axis stabilized satellites has been successfully achieved for several years. The 1990's, however, bring a new challenge to the control problem. Future NASA, military, and commercial space missions will involve advanced space systems which have higher power requirements, greater required pointing accuracies, and faster slewing through larger angular motions. Additionally, permanent space stations, like Freedom, and complex space-platforms, like the Hubble Telescope, will require the use of large, flexible manipulators for maintenance, on-orbit construction, etc.

Research into the demanding problems of the control of flexible structures has been undertaken for the last two decades by major space-system engineering firms, the government laboratories, and universities. The effort has been, however, limited to analytical studies. Recently, experimental work has started at some universities.

Texas A&M University has constructed a hub-appendage configuration to perform large angle maneuvers with vibration suppression for a flexible space vehicle (Junkins, 1989, pp. 1-4). The central hub pivots on a ceramic bearing in the horizontal plane, and four identical cantilevered flexible appendages with endpoint masses protrude from this

2

base. A reaction wheel is driven by a DC brushless motor to provide a system torque. Sensors include an angle encoder, strain gauges and a motor tachometer. Control laws were successfully written to control the system; however, nonlinear friction/stiction occurred as a result of the ceramic bearing, and nonlinear bending moments were observed as a result of the flexibility which hampered accurate modeling of the system response.

Old Dominion University has conducted an experiment to investigate the slewing of flexible structures while simultaneously suppressing vibrational motion during the maneuver (Yang, 1989, pp.1). The experimental setup consists of a trolley on which is mounted a long, flexible beam. The trolley is driven through a driver pulley and a cable transmission system. The flexible beam is rotated in a horizontal plane by the beam motor. Sensors include strain gages, angular potentiometers and a tachometer for the beam motor. Again, nonlinear effects were discovered in large bending deflections, and friction of the cables and trolley, but again they posed no problem in controlling the system.

Stanford University has set up an experiment most similar to the one designed here, and mutual cooperation

between Stanford University and Naval Postgraduate School
has proved invaluable in the early stages of design.

A two link manipulator is used by Stanford University
consisting of two flexible beams pinned at the shoulder, and
joined at the elbow by a limited angle torquer motor
(Oakley,1988, pp. 1-4). Rotary variable differential
transformers measure joint angles, and a CCD television
camera tracks endpoint position. The control equations were
derived using an assumed modes method, and the experimental
results concurred with the simulation. Again, despite
nonlinear effects, accurate modelling was achievable.

At the Naval Postgraduate School, analytical/
experimental studies have been started this year on the
attitude control of flexible spacecraft.

C. EXPERIMENTAL DESIGN

The design of the experimental set-up requires a
compromise between simulation realism and the practicalities
of the hardware. A design is needed that will be an
accurate model for understanding spacecraft control
problems. For this reason, the experiment was constrained
to rotate, not translate, about its principal axis. Pitch
motion is the only motion being investigated and controlled.
In space, a momentum wheel can be used to control pitch axis

motion since the pitch axis is the only axis that remains inertially fixed for Earth-oriented satellites.

There are seven phases of development in the experimental design. This phased approach to building the experimental laboratory allows interim goals to be identified and realized.

1. Phase I

In the initial phase, the design will consist of a mainbody, an L-beam flexible arm, and a reflector (Figure 1). The pitch motion will be controlled by a motor driven momentum wheel. There will be an angle and angular rate sensor on the mainbody. The flexible arm end point position will be measured. Beam mode-shapes will be determined by strain gages and accelerometers.

The mainbody will be controlled with information from the mainbody only. The arm sensors will be utilized for performance measurements and mode shape analysis. The reflector will not be controlled during this phase.

2. Phase II

In phase II, the central body will be controlled with information from the mainbody rate and angular position sensors and the endpoint position sensor.

3. Phase III

A limited-angle stepper motor will be added in phase III at the reflector-arm joint to control the orientation of the reflector with respect to a fixed point on the mainbody.
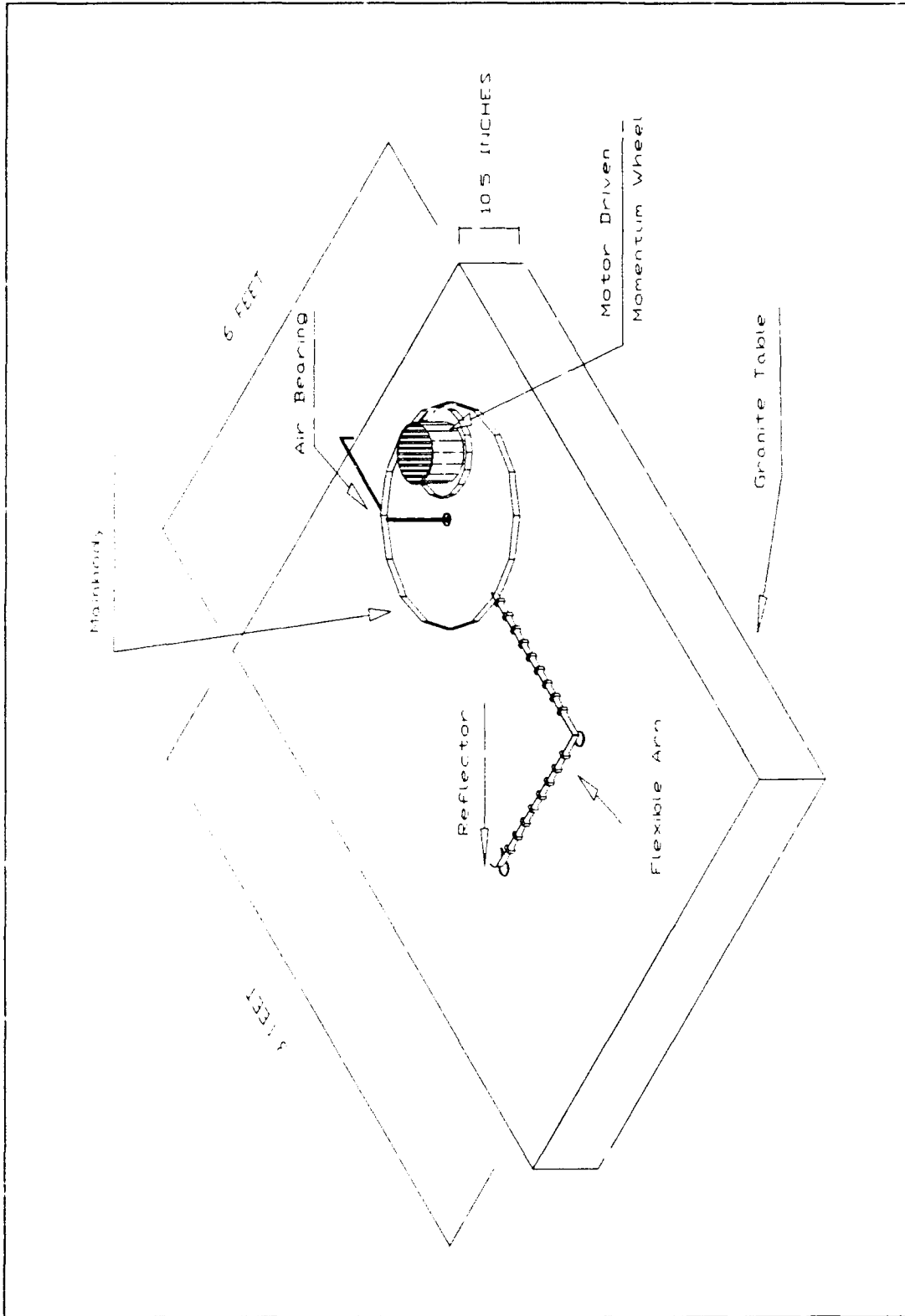
Figure 1 Experimental Set-up.

6

The angular position of the reflector with respect to the end point will be measured. The central body will be controlled, as above. The reflector will also be controlled in both open loop, closed loop with feedback from sensors on the reflector, and closed loop with feedback from all sensors.

4. Phase IV

Thrusters will be added to the mainbody to desaturate the momentum wheel.

5. Phase V

The strain gages and accelerometers will be fed into the control loop for controlling the reflector.

6. Phase VI

Liquid tanks will be added to the system.

7. Phase VII

A limited angle stepper motor and angle position sensor will be added at the L-joint and active control of the flexible arm will be achieved. Eventually, robotics experiments can be explored by fixing the mainbody.

D. OBJECTIVES

This thesis is concerned with the initial design of the experiment through Phase I. There are three main objectives.

1. Experimental Set-up

The preliminary design of the experimental set-up includes the identification of system requirements, the resulting specifications, and the selection of sensors, actuators, and computer systems to make the experiment operational through Phase I.

2. Equations of Motion

The equations of motion for the experimental system must be written to determine the mass and stiffness matrices.

3. System Identification

The system characteristics (the natural frequencies and mode shapes), should be determined by computer aided finite element analysis and verified by experimental modal analysis.

II. EXPERIMENTAL SETUP

The initial design of the experimental set-up consisted of determining the required specifications, researching the available equipment, and selecting the appropriate product. Whenever possible, the set-up was designed as a scaled-down version of existing space-platforms. The specifications were also often based upon real-world considerations, such as acceptable sizes and weights for a laboratory set-up.

A. GRANITE TABLE

Simulation of a space environment requires that gravity and friction be negligible. A large granite table serves as the foundation for the laboratory set-up because precision flatness and smoothness can be achieved.   The mainbody and flexible arm float on air pads that skim over the surface of the granite table.

The table is 6' X 8' X 10.5" and rests on a castor stand. There are set-screws on the metal stand to achieve a level platform. The surface is a Laboratory Grade A .001" finish. The stand has wheels to allow mobility. The table weighs 7550 lbs.

B. MAINBODY

The overall size of the mainbody is constrained by the dimensions of the granite table. In order to have adequate room to maneuver the system when slewing, a 30 inch diameter was chosen.

The base of the mainbody is a simple 7/8" aluminum disk with a 15 inch radius (Figure 2). The mainbody was machined at Naval Postgraduate School by the Aeronautical and Astronautical Engineering department. The top side of the mainbody has seventy two 1/4 inch #20 drilled holes positioned in a radial pattern to allow for a wide assortment of attachments as the experiment grows.
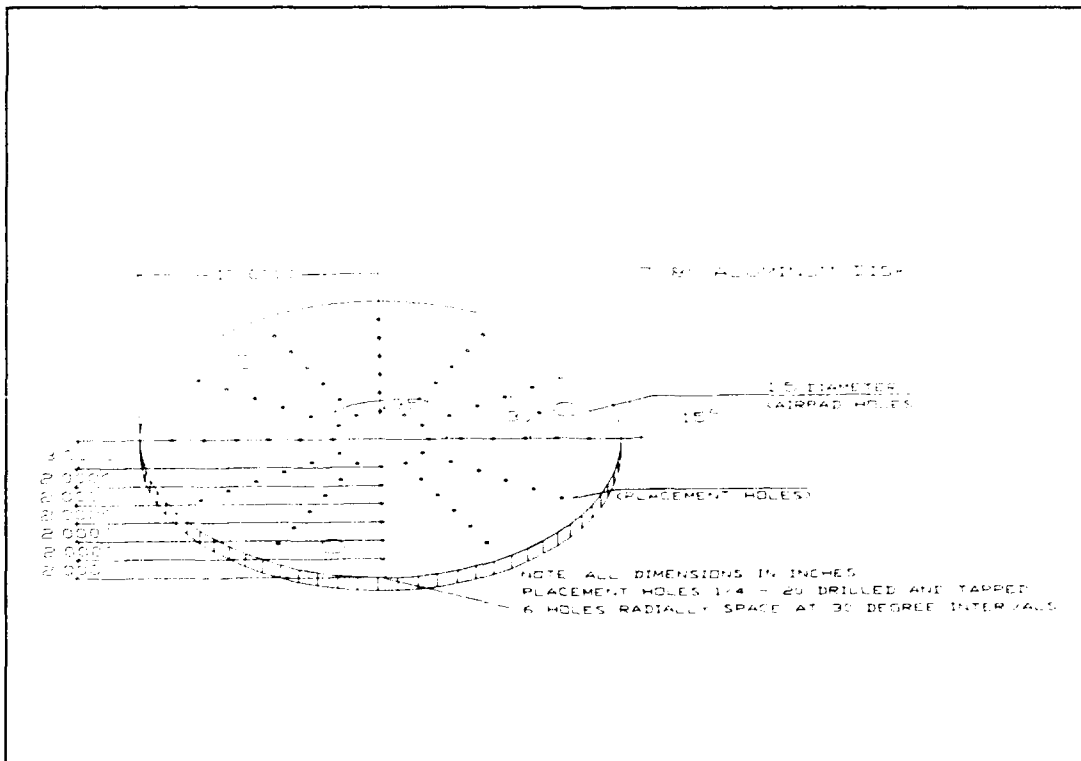

Figure 2 Mainbody Base.

To achieve a realistic simulation of actual spacecraft conditions, the moment of inertia of the mainbody is assumed to be roughly three times the moment of inertia of the flexible arm. From this specification, the moment of inertia of the mainbody can be calculated:

$$I_{mainbody} = (3) \times (I_{arm\ assembly})$$
$$I_{mainbody} = (3) \times 25,000\ lbm\text{-}inches^2 \qquad \textbf{(1)}$$
$$I_{mainbody} = 75,000\ lbm\text{-}inches^2$$

The total mass for the mainbody can be calculated from its moment of inertia:

$$I_{mainbody} = \frac{1}{2}M_{mainbody}r^2_{mainbody} \qquad \textbf{(2)}$$
$$M_{mainbody} = 667\ lbm$$

where $r_{mainbody}$ = 15 inches

For practicality in handling, the mass of the entire mainbody should be under 500 lb. This means that the inertia ratio of flexible assembly/mainbody will be more on the order of 2 to 1, or an I_{mb} of approximately 50,000 lb-in². This gives a total moment of inertia for the entire system of approximately 75,000 lb-in².

The momentum wheel and motor assembly will add approximately 30 lb to the system. From the above

11

calculation, it is obvious that additional weights must be added to the base to achieve the desired moment of inertia.

The mass of the base of the mainbody can be calculated as follows:

$$M_{base} = \rho \pi r_{base}^2 h_{base}$$
$$M_{base} = 59.376 \; lbm \tag{3}$$

where ρ = .096 lb-in^3

r_{base} = 15 inches

h_{base} = 7/8 inches

From the above, the moment of inertia of the base of the mainbody can be calculated by:

$$I_{mb} = \frac{1}{2} M_{mb} r_{mb}$$
$$I_{mb} = 6,679.80 \; lbm\text{-}inches^2 \tag{4}$$

C. FLEXIBLE ARM

The flexible arm (Figure 3) consists of two assemblies of aluminum and steel construction bolted together rigidly in a right angle elbow. Mass intensifiers are connected to the thin (.16 inch) aluminum bar to increase the moment of inertia of the arm assembly without significantly increasing the stiffness. Each mass intensifier (Figure 4) consists of two parts which are bolted together on each side of the aluminum. The tapered design of the mass intensifier

12

reduces the contact between the steel and the aluminum. Minimal contact will ensure greater flexibility.

NOTE: ALUMINUM 6061-T6 BAR
STEEL MASS INTENSIFIERS
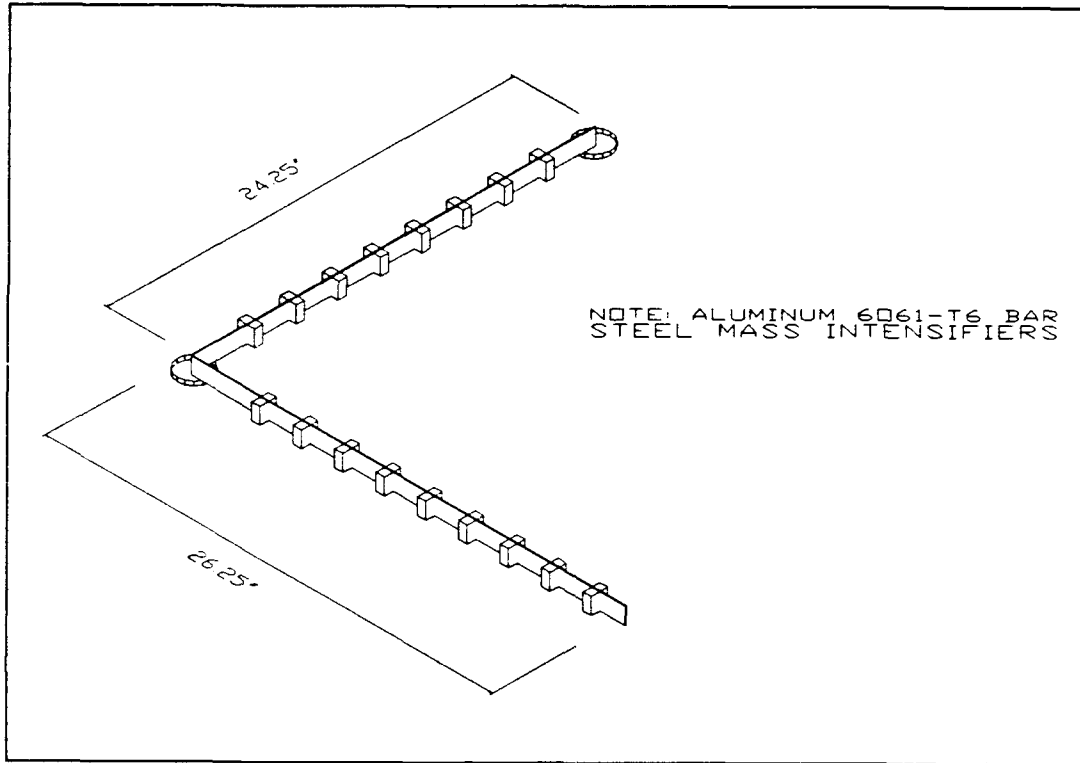
Figure 3 Flexible Arm Assembly.
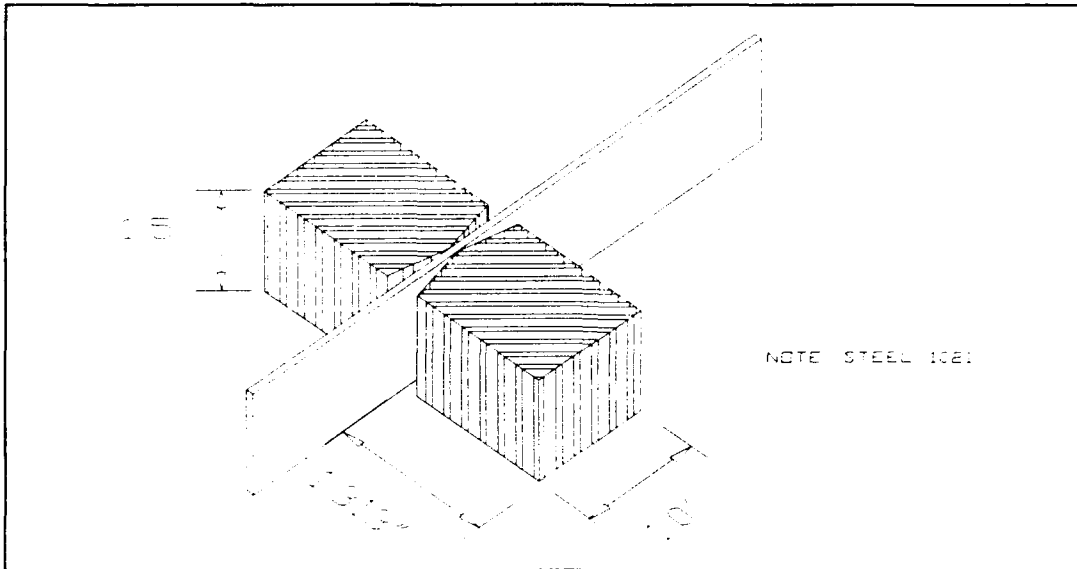
Figure 4 Mass Intensifiers.

The elbow joint consists of two aluminum right angle braces connected to a circular aluminum disk. The end joint has an aluminum wedge bolted to a circular aluminum disk. This wedge shape allows free motion of the endpoint. The end of the flexible arm will house a reflector and will be the location for end point sensing.

The total mass of the flexible arm assembly can be calculated as follows:

$$mass\ of\ aluminum\ rod_A = .411\ lbm$$
$$mass\ of\ aluminum\ rod_B = .380\ lbm$$
$$mass\ of\ each\ intensifier\ pair = 1.056\ lbm$$

$$Total\ mass\ of\ arm_A = 9.66\ lbm$$
$$Total\ mass\ of\ arm_B = 8.59\ lbm \qquad \textbf{(5)}$$

$$mass\ of\ elbow\ joint = .244\ lbm$$
$$mass\ of\ end\ joint = .183\ lbm$$

$$Total\ mass\ of\ flexible\ assembly = 18.68\ lbm$$

The center of mass of the flexible arm assembly is:

$$\text{Center of mass of } arm_A = \frac{\sum m_{Ai} r_{Ai}}{M_{arm_A}}$$

$$CM_{arm_A} = 12.96 \text{ inches } \hat{i}$$

$$\text{Center of mass of } arm_B = \frac{\sum m_{Bi} r_{Bi}}{M_{arm_B}}$$

$$CM_{arm_B} = 11.66 \text{ inches } \hat{j}$$

$$\text{Center of mass of arm assembly} = \frac{\sum m_{cm} r_{cm}}{M} \tag{6}$$

$$CM(x)_{assembly} = \frac{M_{arm_A} CM_{arm_A}(x) + M_{arm_B} CM_{arm_B}(x)}{M_{arm_A} + M_{arm_B}}$$

$$CM(y)_{assembly} = \frac{M_{arm_A} CM_{arm_A}(y) + M_{arm_B} CM_{arm_B}(y)}{M_{arm_A} + M_{arm_B}}$$

$$CM(x)_{assembly} = 19.29 \text{ inches}$$
$$CM(y)_{assembly} = 5.55 \text{ inches}$$

The moment of inertia of each arm can be calculated about the center of mass of each arm. Each mass intensifier and the elbow and end joint braces are computed as point masses. The moment of inertia for the flexible arm assembly can be calculated about the origin O by the parallel axis theorem.

$$(I_{CM_{arm_A}}) = \sum m_{Ai} r_{Ai}^2$$
$$(I_{CM_{arm_A}}) = 416.10 \; lbm\text{-}inches^2$$

$$(I_{CM_{arm_B}}) = \sum m_{Bi} r_{Ai}^2$$
$$(I_{CM_{arm_B}}) = 324.03 \; lbm\text{-}inches^2$$

$$(I_{arm_{A_O}}) = I_{CM_{arm_A}} + d^2 \, M_{arm_A}$$

$$\text{where } d = (15+12.96) = 27.96 \; inches$$

$$(I_{arm_{A_O}}) = 7,967.92 \; lbm\text{-}inches^2 \tag{7}$$

$$(I_{arm_{B_O}}) = I_{CM_{arm_B}} + d^2 \, M_{arm_B}$$

$$\text{where } d = \sqrt{(15 + 27.96)^2 + (11.66)^2} = 42.85 \; inches$$

$$(I_{arm_{B_O}}) = 16,096.32 \; lbm\text{-}inches^2$$

$$I_{arm\;assembly_O} = I_{arm_{A_O}} + I_{arm_{B_O}}$$

$$I_{arm\;assembly_O} = 24,064.24 \; lbm\text{-}inches^2$$

D. MOMENTUM WHEEL

A motor driven momentum wheel will be used to apply a torque (the change in the angular momentum) for slewing the mainbody.

For preliminary calculations, a one foot diameter aluminum disk with one inch thickness can be used for the dimensions of the momentum wheel.

The mass of the momentum wheel can be calculated as:

$$m_{mw} = \rho \, \pi \, r_{mw}^2 \, h_{mw}$$

$$
\begin{aligned}
where \quad r_{mw} &= 6.00 \; inches \\
h_{mw} &= 1.0 \; inches \\
\rho &= .096 \; \frac{lbm}{inches^3} \\
m_{mw} &= 10.857 \; lbm
\end{aligned}
\qquad (8)
$$

The moment of inertia for the momentum wheel is:

$$I_{mw} = \frac{1}{2} m_{mw} \, r_{mw}^2$$

$$
\begin{aligned}
where \quad r_{mw} &= 6.00 \; inches \\
m_{mw} &= 10.857 \; lbm \\
I_{mw} &= 195.43 \; lbm\text{-}inches^2 \\
I_{mw} &= 8.094 \; oz\text{-}inches\text{-}sec^2
\end{aligned}
\qquad (9)
$$

E. TORQUE MOTOR

The momentum wheel must be driven by a motor that will deliver the required change in angular momentum to the system. A specification for the system design, based upon existing space platforms, is that the mainbody accelerate at the rate of 12 degrees per second^2.

From this specification, the torque of the motor can be determined to be:

$$I_{system} \alpha_{system} = I_{mw} \alpha_{mw}$$

$$(3000oz\text{-}inches\text{-}sec^2)(.209\frac{rad}{sec^2}) = (8.094oz\text{-}inches\text{-}sec^2)(\alpha_{mw})$$

$$\alpha_{mw} = 80 \frac{rad}{sec^2} \qquad \textbf{(10)}$$

$$Torque \ of \ momentum \ wheel = I_{mw} \ \alpha_{mw}$$

$$T_{mw} = 650 \ oz\text{-}inch$$

$$T_{mw} = 4.59 \ N\text{-}m$$

From the above calculation, the momentum wheel must apply a 650 oz-inch (4.59 N-m) torque to provide the desired slew rate for the mainbody.

The motor selected was a DC servo-disc motor. In the servo-disc motor, the ironless armature is constructed from several layers of copper conductors in a flat-disc configuration. This allows for low inertia and fast acceleration. Additionally, the smaller size can be easily mounted on the mainbody. Table I outlines the motor characteristic.

18

TABLE I PMI SERVO-DISC MOTOR		
Motor Performance	Units	TR16M4C
Peak Torque	oz-in	5307.2
Continuous Stall Torque	oz-in	498.4
Peak Current	Amps	100.8
Peak Acceleration w/o Load	KRADS/sec^2	63.2
Horsepower	HP	1.4
Torque	oz-in	473.4
Speed	RPM	3000
Power Output	Watts	1049.5
Terminal Voltage	Volts	128.7
Current	Amps	9.55
Torque Constant (KT)	oz-in/	52.77
Motor Weight	Lb	17.50
Moment of Inertia	oz-in-s^2	.084
Cost (includes tachometer)	ea	$1229.0

The motor will be aligned in a vertical position on top of the momentum wheel to deliver a torque about the vertical (pitch) axis. The motor housing includes an attachment shaft for fitting with the momentum wheel.

F. SENSORS

Initially, the angular position and the angular rate of the mainbody and the speed of the momentum wheel will be sensed. At a later time, the angular position of the reflector with respect to the endpoint, and the position of the endpoint with respect to the mainbody, will be measured.

The angular rate of the torquer motor and momentum wheel will be sensed by a tachometer which is attached to the motor. Table II outlines the tachometer characteristics.

TABLE II PMI TACHOMETER		
Tachometer Performance	Units	JR16M4CH
Maximum Speed	RPM	4000
Bidirectional Tolerance	%V	± 1.5
Tachometer Weight	lb	2.2
Moment of Inertia	oz-in-s^2	.005

The angular rate of the mainbody will be monitored by a rate sensing gyroscope. The gyroscope produces an analog output voltage proportional to the angular velocity about the sensing axis (in this case, the Z axis at the origin).

When a rotation exists, the Coriolis forces transfer momentum to the perpendicular plane and cause a bending of the solid state sensing elements. These elements will vibrate 180 degrees out of phase with angular motion but in phase when linear acceleration or vibration occurs. The integrated electronics produce an angular motion response output with no linear motion incorporated. A single axis gyroscope with a range of ±30 degrees per second was selected. Table III shows the rate gyroscope characteristics.

TABLE III WATSON RATE GYROSCOPE		
Rate Gyroscope	Units	ARS-C121-1A
Output	VDC	0 at zero angular rate ±10 at full scale angular rate
Power Supply	VDC	$\pm$ 15 $\pm$ 5% 20 mA maximum
Range	degree /sec	$\pm$ 30
Weight	Oz	4
Cost	ea	$ 802.00

Angular position for both the mainbody and the endpoint reflector will be measured by rotary variable differential transformers (RVDTs). RVDTs measure the angular displacement of rotating elements by producing a voltage whose magnitude varies linearly with the angular position of the shaft. The RVDT is constructed on precision ball

bearings to minimize friction and noise. The best operating range of a RVDT is $\pm$ 40 degrees, which is well within the confines of this experiment. The characteristics of the RVDTs purchased are in Table IV.

TABLE IV SCHAEVITZ ROTARY VARIABLE DIFFERENTIAL TRANSFORMER		
RVDTs	Units	R30D
Linearity	% of range	$\pm$ 30° : .25 $\pm$ 40° : .50 $\pm$ 60° : 1.5
Moment of Inertia	Oz-in-sec^{2}	8.5 x 10^{-6}
Maximum Torque	Inch-oz	.019
Maximum Load	Lb	Radial = 8 Axial = 10
Weight	Oz	1.87
Cost	ea	$438.00

Endpoint sensing has yet to be determined. The accuracies required ($\pm$ .1 mm) over the large span of control ($\pm$ 5 cm) make most conventional endpoint sensing techniques inadequate. CCD cameras would provide the required coverage area, however they would give only 1 mm accuracies and the

signal processing equipment required to integrate CCD cameras into the control loop would be expansive. Greater accuracies can easily be achieved by off-the-shelf capacitance sensors, however the coverage area would be much smaller than that required by this experiment.

A promising devise for lateral position sensing is the electro-optical photodetector. Using a fixed-position laser or LED light source, a mirror system and a photodiode receiver collect the reflected light and provide an output signal proportional to the position.

Standard off-the-shelf units can be purchased through several sources. The unit would consist of an analog optical position monitor (approximate cost $3,500) and a detector/cable assembly (approximate cost $400).

G. AIR PADS

The mainbody and the flexible arm will be supported by five aluminum air pads, each capable of supporting a 60 lb load. Each pad is fed by 80 PSI of air, which is regulated by two regulators. One regulator feeds the three mainbody air pads, and one regulator feeds the elbow and endpoint air pads.

On the mainbody, three 1.5 inch diameter mounting holes are located 120 degrees apart three inches from the outer edge. The air feed is on the side of each pad. A top brace will be fashioned and mounted to the mainbody to hold the air pads in place. Three air pads for the mainbody have

been chosen as the optimum number for controlling the mass. An odd number of pads decreases the likelihood of leverage effects due to uneven load distributions. A 150 psi regulator will control all three mainbody air pads. The 150 psi regulator was chosen to allow upgrades to larger air pads at a later date.

H. AIR BEARING

The entire system will be constrained to rotational motion only by an air bearing mounted to the center of the mainbody from above. Translational motion will be constrained in the initial phase of the experiment so that pitch effects can be isolated. At a later time, the air bearing can be removed so that robotics experiments can be performed. The air bearing (Figure 5) consists of an H-type bearing which is capable of carrying both a radial and an axial load. As the mass of the mainbody is increased, the air bearing can be used to support some of the load. A mounting bracket will be attached to the side of the granite table and will be connected to the mainbody from above.
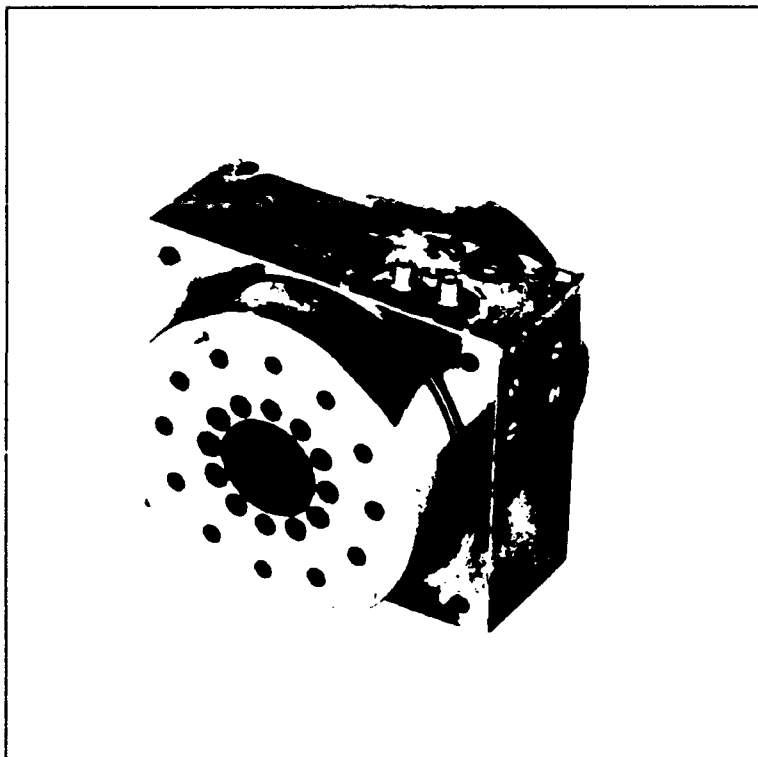
Figure 5 Air Bearing.

I. COMPUTER SYSTEM

The AC-100 computer system, manufactured by Integrated Systems, Inc., has been purchased to provide data acquisition and results analysis for the experimental set-up. The AC-100 is an automatically-programmable real-time control system that will allow graphical specification and simulation of real-time systems. This will allow the experimental set-up to be fully monitored real-time from the workstation.

The AC-100 system consists of three parts: the workstation, the AC-100 software, and the AC-100 controller.

25

The workstation includes a DEC 3100 computer, VMS operating system, 8 MB RAM memory, two 105 MB hard disks, a 19 inch color monitor and an Ethernet interface. PWS003 modeling, simulation and implementation software are combined with a VAX C and VAX Fortran compiler. The controller has 16 channel inputs and 10 channel outputs in addition to 32 parallel digital inputs/outputs, eight encoder inputs, and one event trigger input.

III. EXPERIMENTAL ANALYSIS

A. MODAL ANALYSIS

Experimental modal testing can be conducted to determine
the nature of the vibration response and to verify the
analytical models. The Hewlett-Packard VISTA Data
Acquisition Package was used to collect information
concerning the time and frequency response of the flexible
arm assembly in a free-free mode.

The frequency response function method of modal testing
requires that the input excitation and the output response
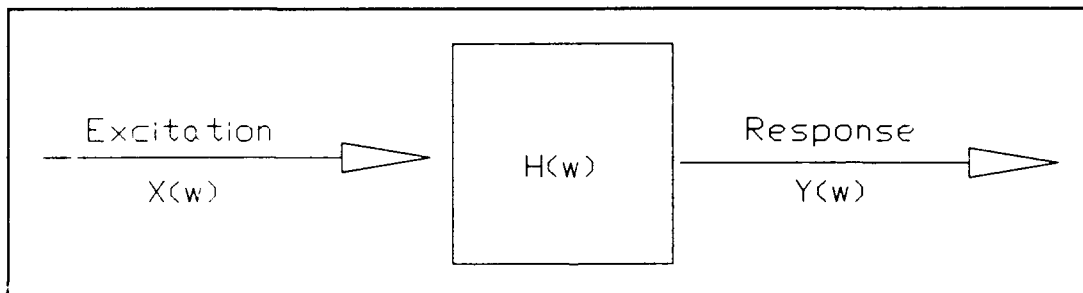be measured simultanously to determine the system function
(Figure 6).

Figure 6   System Block Diagram.

The VISTA program utilizes a dynamic signal analyzer,
which is a Fourier transform-based instrument, to process
the measurements of the structures frequency response
(Hewlett- Packard, 1986, pp. 11).

The input used was a single-point excitation impact hammer. The hammer is the most simple way to excite a structure into vibration. The exciter consists of an impactor, with several different tips and heads which will allow some flexibility in setting the force level ranges for testing different objects (Ewins, 1984, pp. 102-104). The hammer contains an ICP quartz force sensor mounted on the striking end of the hammer (PCB Piezotronics, 1983, pp. 1). The impact force is transferred via the sensing element into an electrical signal which can be evaluated.

The hammer impulse consists of a nearly constant force over a wide frequency range and therefore can excite all resonances in that range. The size of the hammer, along with the hammer tip material and velocity, determine the amplitude of the force impulse. The frequency content of the energy applied to the arm is a function of the stiffness of the contacting surfaces and the mass of the hammer. The hammer tip selected affects the force impulse, and therefore the frequency response. A hard, steel tip was selected to deliver a short pulse duration and higher frequency content.

The flexible arm assembly was supported from above by small soft elastic cords in an attempt to simulate the free-free mode (Figure 7). An ICP accelerometer was positioned in the XY plane at the end of each arm. When the accelerometer vibrates, an internal mass applies a force to the crystal element which is proportional to the

28

acceleration. Using Newton's Law, the resulting force output can be measured.
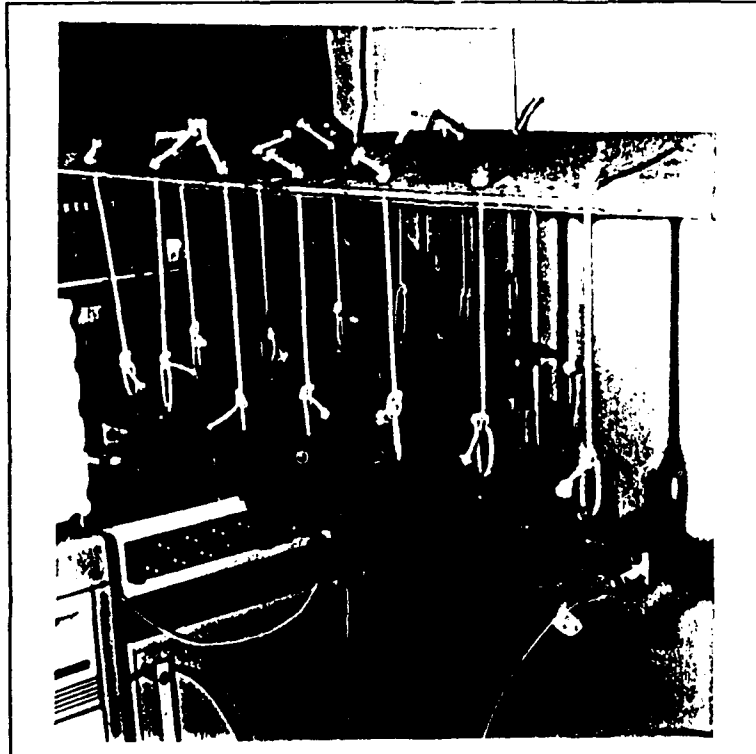

Figure 7   Flexible Arm Assembly Support.

The assembly was struck with the hammer in various places throughout the assembly. The resulting frequency response showed consistent modes of varying amplitudes, depending upon where the structure was struck.

Figure 8 shows the time and frequency spectrum for the impact hammer as struck about midway on arm A. Figure 9 and Figure 10 show the time and frequency measurements for each arm as a result of the impact.
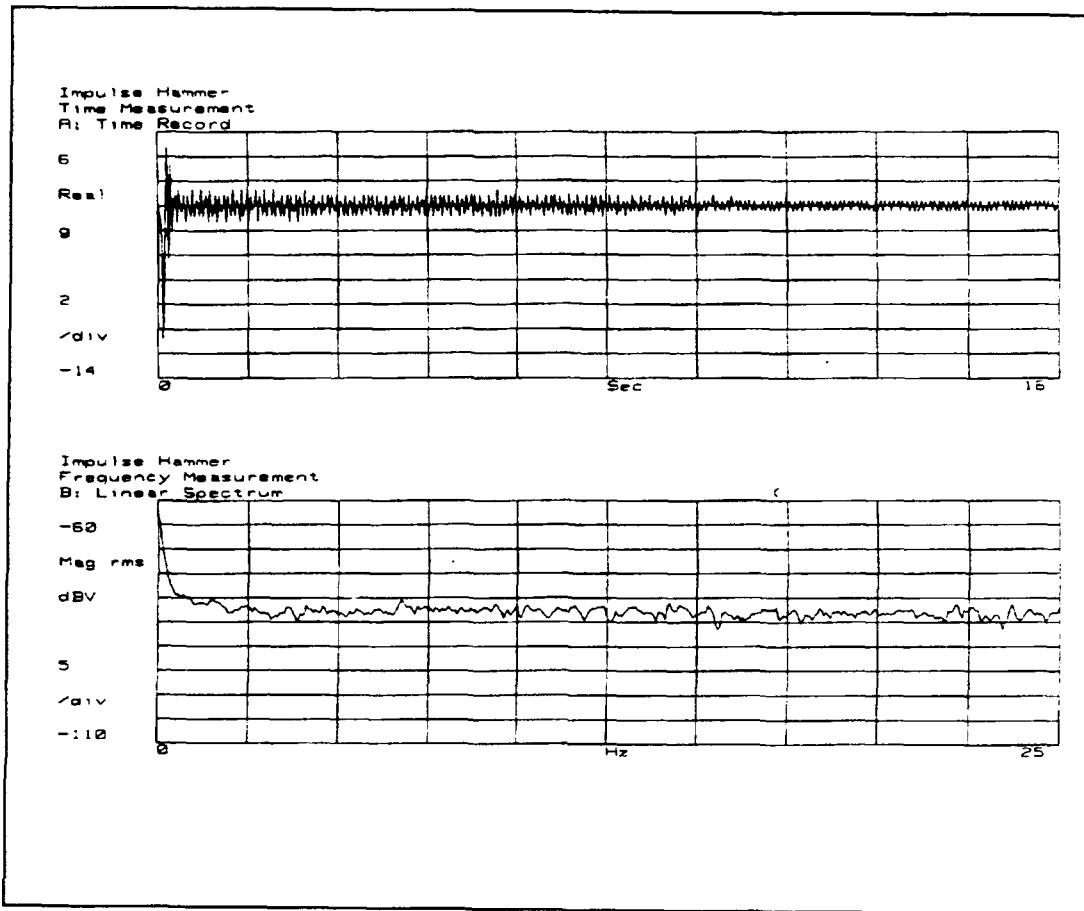
29

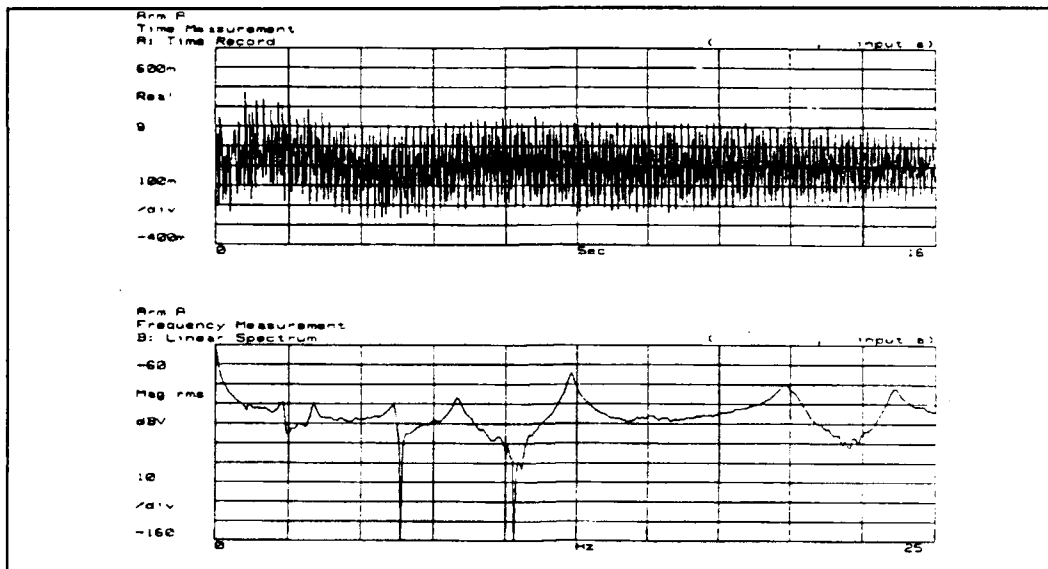**Figure 8 Impact Hammer Time and Frequency Measurements.**

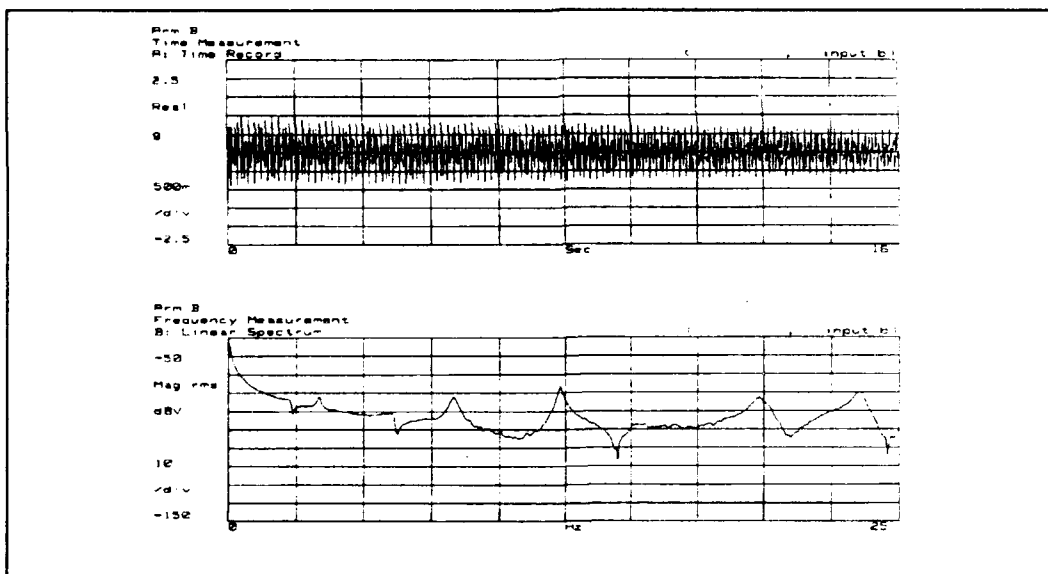**Figure 9 Arm A Time and Frequency Response.**

Figure 10 Arm B Time and Frequency Measurement.

31

The finite element analysis was evaluated for the free-free condition, and the mode frequencies were computed. When compared with the experimental results, a fairly good correlation was found between the two, with the exception of the first mode. Table V shows the difference between the frequencies obtained from the GIFTS program and the experimental values.

TABLE V FINITE ELEMENT ANALYSIS VS. EXPERIMENTAL RESULTS			
MODE	GIFTS Hz	EXP.AVG Hz	DIFFER-ENCE Hz
1	.548	1.125	-.577
2	2.087	2.249	-.162
3	3.057	3.375	-.318
4	6.483	6.093	.390
5	8.133	8.312	-.179
6	13.424	12.313	1.111
7	15.667	15.125	.542

IV. THEORETICAL ANALYSIS

A. EQUATIONS OF MOTION

The system equations of motion can be derived as a
mathematical model for the experimental set-up. This model
is based upon given physical laws which govern the system
behavior, such as force-deformation relationships and the
laws of motion. The equations of motion will identify the
mass and stiffness system parameters.

In a "lumped-parameter" system, the equations are a
function of time alone, which are ordinary differential
equations and are easy to solve (Meirovitch, 1990, pp. 45-
53). In the "distributed-system-parameter" system, the
equations are functions of both spatial coordinates and
time, and are therefore partial differential equations which
can not be easily solved. Therefore, a discret model must
be devised to model the distributed system.

A flexible system is a non-linear system. In other
words, the response of the experimental set-up to different
excitations can not be obtained separately and combined
linearly. Nonlinearity may present complications in
modelling and control. A careful comparison of the
analytical verses experimental results will identify
nonlinear variations.

The equations of motion for a flexible structure can be written as a function of spatial variables, which can be assumed as known, and unknown time variables. This will result in a discrete model containing ordinary differential equations. The solution can be represented as spatial eigenfunctions multiplied by time-dependant generalized coordinates.

Lagrange's equation facilitates writing the equations of motion for a flexible multiple degree of freedom system. Additionally, Lagrange's technique produces an entirely scalar process using the quantities of potential energy, kinetic energy, and work in terms of a generalized coordinate system (Meirovitch, 1967, pp.47-59).

The Lagrange Operator is:

$$\frac{d}{dt} \left(\frac{\partial L}{\partial \dot{q}_i} \right) - \frac{\partial L}{\partial q_i} - \phi \qquad (17.)$$

where L is the Lagrangian: T - V

T = System kinetic energy

V = System potential energy

q_i = System generalized coordinates

ϕ = System generalized force

34

By using this method of analysis, the complicated dynamic problem can be reduced to a scalar integral that does not depend on the coordinates used.

The kinetic energy of a distributed system is:

$$T = \int_S \frac{1}{2} \rho \, (V_O)^2 \, ds \qquad (12)$$

where ρ is the material density, V_0 is the velocity of a generic point of the system in inertial frame

The origin O for the experimental set-up was chosen to be the center of the mainbody. This is the point where the mainbody is attached to the air bearing (Figure 11). This origin O is therefore fixed in the reference frame of the table.

The value of V_0 can be determined from the following formula:

$$\vec{V}_O = \vec{V}_p + \vec{\omega} \times \vec{r}_{o-p} \qquad (13)$$
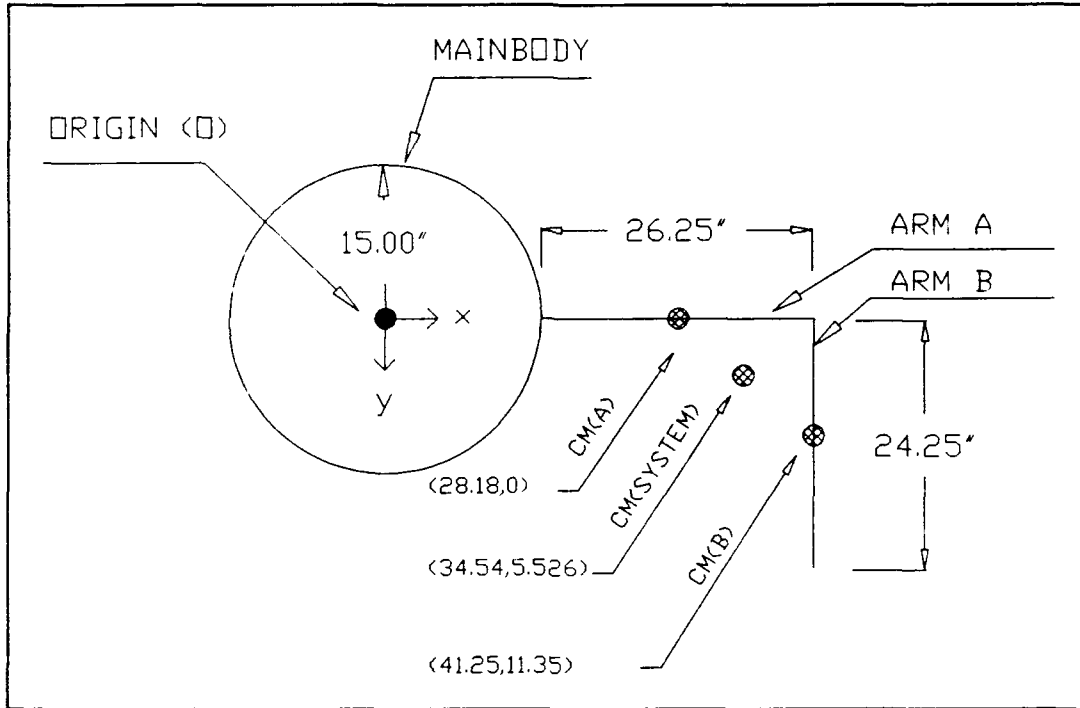$$\text{where } \dot{\omega} = \dot{\theta} \, \hat{k}$$

Figure 11 Experimental Set-up.

The position vector from the origin O to any point on the arm can be described by:

$$\bar{r}_{0\text{-}a} = x\ \hat{i} + W_a\ \hat{j}$$

$$r_{0\text{-}b} = (R+L_1+W_b)\ \hat{i} + (W_{ae} + y)\ \hat{j}$$

where L_1 = length of Arm A

R = radius of the mainbody

W_{ae} = the vertical endpoint displacement of Arm A

thus

$$\vec{\omega} \times \vec{r}_{0\text{-}a} = \theta\hat{k} \times [(X\hat{i}+W_a\hat{j})] = -W_a\theta\hat{i}+X\theta\hat{j}$$
$$\vec{\omega} \times \vec{r}_{0\text{-}b} = \theta\hat{k} \times [(R+L_1+W_b)\ \hat{i} + (Y+W_{ae})\ \hat{j}] \qquad \textbf{(14)}$$
$$= (-W_{ae}\theta - Y\theta)\ \hat{i} + (R+L_1+W_b)\theta\ \hat{j}$$

Using the function $W_a(x,y,t)$ to represent the position of any arbitrary point on beam A, and $W_b(x,y,t)$ to represent the position of any arbitrary point on beam B:

$$W_a = \psi_{a1}(x)\,q_1(t) + \psi_{a2}(x)\,q_2(t)$$
$$W_b = \psi_{b1}(y)\,q_1(t) + \psi_{b2}(y)\,q_2(t)$$
$$W_{ae} = \psi_{a1}(L_1)\,q_1(t) + \psi_{a2}(L_2)\,q_2(t) \qquad \textbf{(15)}$$
$$= \beta_1\,q_1(t) + \beta_2\,q_2(t)$$

where ψ is a function of spatial variables only and q(t) is the time dependant general coordinate

37

The subscripts 1 and 2 refer to the first and second modes of the structure. Only the first two modes have been incorporated in the spatial equations, but others could easily be added at a later time. The displacement in X direction for Arm A has been ignored as insignificant compared to the other displacements.

Substituting this new variable into the equation, the kinetic energy of the system can be calculated to be:

$$KEsystem = \frac{1}{2} I_{mb} \; \dot\theta^2 +$$

$$[\frac{\rho}{2}\int_0^{L_2}\beta_1^2 dy + \frac{\rho}{2}\int_R^{R+L_1}\psi_{a1}^2 dx + \frac{\rho}{2}\int_0^{L_2}\psi_{b1}^2 dy] \; q_1^2\dot\theta^2 +$$

$$[\rho\int_0^{L_2}\beta_1\beta_2 dy + \rho\int_R^{R+L_1}\psi_{a1}\psi_{a2} dx + \rho\int_0^{L_2}\psi_{b1}\psi_{b2} dy] \; q_1 q_2\dot\theta^2 +$$

$$[\frac{\rho}{2}\int_0^{L_2}\beta_2^2 dy + \frac{\rho}{2}\int_R^{R+L_1}\psi_{a2}^2 dx + \frac{\rho}{2}\int_0^{L_2}\psi_{b2}^2 dy] \; q_2^2\dot\theta^2 +$$

$$[\frac{\rho}{2}\beta_1^2 L_2 + \frac{\rho}{2}\int_R^{R+L_1}\psi_{a1}^2 dx + \frac{\rho}{2}\int_0^{L_2}\psi_{b1}^2 dy] \; \dot q_1^2 +$$

$$[\rho\beta_1\beta_2 L_2 + \rho\int_R^{R+L_1}\psi_{a1}\psi_{a2} dx + \rho\int_0^{L_2}\psi_{b1}\psi_{b2} dy] \; \dot q_1\dot q_2 +$$

$$[\rho(R+L_1)L_2\beta_1 + \rho\int_R^{R+L_1}X\psi_{a1} dx - \rho\int_0^{L_2}Y\psi_{b1} dy] \; \dot q_1\dot\theta +$$

$$[\rho\beta_2^2 L_2 + \frac{\rho}{2}\int_R^{R+L_1}\psi_{a2}^2 dx + \frac{\rho}{2}\int_0^{L_2}\psi_{b2}^2 dy] \; \dot q_2^2 + \qquad (16)$$

$$[\rho(R_1+L_1)L_2\beta_2 + \rho\int_R^{R+L_1}x\psi_{a2} dx - \rho\int_0^{L_2}y\psi_{b2} dy] \; \dot q_2\dot\theta +$$

$$[\frac{\rho}{2}\int_R^{R+L_1}x^2 dx + \frac{\rho}{2}\int_0^{L_2}y^2 + (R+L_1)^2 dy] \; \dot\theta^2 +$$

$$[\rho\int_0^{L_2}(R+L_1)\psi_{b1} dy] \; q_1\dot\theta^2 + [\rho\int_0^{L_2}(R+L_1)\psi_{b2} dy] \; q_2\dot\theta^2 -$$

$$[\rho\int_0^{L_2}\beta_2\psi_{b1} dy] \; \dot q_1 q_2\dot\theta - [\rho\int_0^{L_2}\beta_2\psi_{b2} dy] \; q_2\dot q_2\dot\theta +$$

$$[\rho\int_0^{L_2}\beta_2 Y dy] \; q_2\dot\theta^2 + [\rho\int_0^{L_2}\beta_1 Y dy] \; q_1\dot\theta^2 -$$

$$[\rho\int_0^{L_2}\beta_1\psi_{b2} dy] \; q_1\dot q_2\dot\theta - [\rho\int_0^{L_2}\beta_1\psi_{b1} dy] \; q_1\dot q_1\dot\theta$$

The potential energy of the system is the flexural strain energy. To calculate the potential energy of each beam, the following equation can be used:

$$U = \frac{1}{2} \int_{R}^{R+L_1} EI \left(\frac{d^2 W_a}{dx^2} \right)^2 dx + \qquad (12)$$
$$\frac{1}{2} \int_{0}^{L_2} EI \left(\frac{d^2 W_b}{dy^2} \right)^2 dy$$

Substituting the expressions for W_a, W_{ae}, and W_b into this equation, the total potential energy of the system is calculated.

The rotary inertia effect and the axial deformation effect on the potential energy have been ignored. The cross-sectional dimensions are small compared to the length of the bar.

The Lagrangian can now be written in the following form:

$$[\frac{1}{2}I_{mb}+\frac{\rho}{2}\int_{R}^{R+L_1}X^2dx+\frac{\rho}{2}\int_{0}^{L_2}Y^2+(R+L_1)^2dy]\ \theta^2\ +$$

$$[\frac{\rho}{2}\int_{0}^{L_2}\beta_1^2dy+\frac{\rho}{2}\int_{R}^{R+L_1}\psi_{a1}^2dx+\frac{\rho}{2}\int_{0}^{L_2}\psi_{b1}^2dy]\ q_1^2\theta^2\ +$$

$$[\rho\int_{0}^{L_1}\beta_1\beta_2dy+\rho\int_{R}^{R+L_1}\psi_{a1}\psi_{a2}dx+\rho\int_{0}^{L_2}\psi_{b1}\psi_{b2}dy]\ q_1q_2\theta^2\ +$$

$$[\frac{\rho}{2}\int_{0}^{L_2}\beta_2^2dy+\frac{\rho}{2}\int_{R}^{R+L_1}\psi_{a2}^2dx+\frac{\rho}{2}\int_{0}^{L_2}\psi_{b2}^2dy]\ q_2^2\theta^2\ +$$

$$[\frac{\rho}{2}\beta_1^2L_2+\frac{\rho}{2}\int_{R}^{R+L_1}\psi_{a1}^2dx+\frac{\rho}{2}\int_{0}^{L_2}\psi_{b1}^2dy]\ \dot{q}_1^2\ +$$

$$[\rho\beta_1\beta_2L_2+\rho\int_{R}^{R+L_1}\psi_{a1}\psi_{a2}dx+\rho\int_{0}^{L_2}\psi_{b1}\psi_{b2}dy]\ \dot{q}_1\dot{q}_2\ +$$

$$[\rho(R+L_1)L_2\beta_1+\rho\int_{R}^{R+L_1}X\psi_{a1}dx-\rho\int_{0}^{L_2}Y\psi_{b1}dy]\ \dot{q}_1\theta\ +$$

$$[\frac{\rho}{2}\beta_2^2L_2+\frac{\rho}{2}\int_{R}^{R+L_1}\psi_{a2}^2dx+\frac{\rho}{2}\int_{0}^{L_2}\psi_{b2}^2dy]\ \dot{q}_2^2\ +$$

(18)

$$[\rho(R+L_1)L_2\beta_2+\rho\int_{R}^{R+L_1}X\psi_{a2}dx-\rho\int_{0}^{L_2}y\psi_{b2}dy]\ \dot{q}_2\theta\ +$$

$$[\rho\int_{0}^{L_2}(R+L_1)\psi_{b1}dy]\ q_1\theta^2+[\rho\int_{0}^{L_2}(R+L_1)\psi_{b2}dy]\ q_2\theta^2\ -$$

$$[\rho\int_{0}^{L_2}\psi_{b1}\beta_2dy]\ \dot{q}_1q_2\theta\ -\ \rho\int_{0}^{L_2}\beta_2\psi_{b2}dy]\ q_2\dot{q}_2\theta\ +$$

$$[\rho\int_{0}^{L_2}\beta_2Ydy]\ q_2\theta^2\ +\ [\rho\int_{0}^{L_2}\beta_1Ydy]\ q_1\theta^2\ -$$

$$[\rho\int_{0}^{L_2}\psi_{b2}\beta_1dy]\ q_1\dot{q}_2\theta\ -\ [\rho\int_{0}^{L_2}\psi_{b1}\beta_1dy]\ q_1\dot{q}_1\theta\ -$$

$$[\frac{EI}{2}\int_{R}^{R+L_1}(\frac{d^2\psi_{a1}}{dx^2})^2dx+\frac{EI}{2}\int_{0}^{L_2}(\frac{d^2\psi_{b1}}{dy^2})^2dy]\ q_1^2\ -$$

$$[EI\int_{R}^{R+L_1}(\frac{d^2\psi_{a1}}{dx^2}\frac{d^2\psi_{a2}}{dx^2})dx+EI\int_{0}^{L_2}(\frac{d^2\psi_{b1}}{dy^2}\frac{d^2\psi_{b2}}{dy^2})dy]\ q_1q_2\ -$$

$$[\frac{EI}{2}\int_{R}^{R+L_1}(\frac{d^2\psi_{a2}}{dx^2})^2dx+\frac{EI}{2}\int_{0}^{L_2}(\frac{d^2\psi_{b2}}{dy^2})^2dy]\ q_2^2$$

41

Performing the Lagrangian Operator, the resulting matrix is as follows:

$$
\begin{vmatrix} M11 & M12 & M13 \\ M21 & M22 & M23 \\ M31 & M32 & M33 \end{vmatrix}
\begin{vmatrix} \ddot{q}_1 \\ \ddot{q}_2 \\ \ddot{\theta} \end{vmatrix}
+
\begin{vmatrix} K11 & K12 & K13 \\ K21 & K22 & K23 \\ K31 & K32 & K33 \end{vmatrix}
\begin{vmatrix} q_1 \\ g_2 \\ \theta \end{vmatrix}
+
\begin{vmatrix} V_1 \\ V_2 \\ V_3 \end{vmatrix}
=
\begin{vmatrix} 0 \\ 0 \\ \Phi \end{vmatrix}
\qquad (19)
$$

where :

$$
M11 = \rho \int_R^{R+L_1} \psi_{a1}^2 dx + \rho \int_0^{L_2} \psi_{b1}^2 dy + \rho L_2 \beta_1^2
$$

$$
M12 = \rho \int_R^{R+L_1} \psi_{a1}\psi_{a2} dx - \rho \int_0^{L_2} \psi_{b1}\psi_{b2} dy + \rho L_2 \beta_1 \beta_2
$$

$$
M13 = \rho \int_R^{R+L_1} X\psi_{a1} dx - \rho \int_0^{L_2} Y\psi_{b1} dy + \frac{\rho}{2}(R+L_1) L_2 \beta_1
$$

$$
M21 = \rho \int_R^{R+L_1} \psi_{a1}\psi_{a2} dx - \rho \int_0^{L_2} \psi_{b1}\psi_{b2} dy + \rho L_2 \beta_1 \beta_2
$$

$$
M22 = \rho \int_R^{R+L_1} \psi_{a2}^2 dx + \rho \int_0^{L_2} \psi_{b2}^2 dy + \rho L_2 \beta_1^2 \qquad (20)
$$

$$
M23 = \rho \int_R^{R+L_1} X\psi_{a2} dx - \rho \int_0^{L_2} Y\psi_{b2} dy + \frac{\rho}{2}(R+L_1) L_2 \beta_2
$$

$$
M31 = \rho \int_R^{R+L_1} X\psi_{a1} dx - \rho \int_0^{L_2} Y\psi_{b1} dy + \frac{\rho}{2}(R+L_1) L_2 \beta_1
$$

$$
M32 = \rho \int_R^{R+L_1} X\psi_{a2} dx - \rho \int_0^{L_2} Y\psi_{b2} dy + \frac{\rho}{2}(R+L_1) L_2 \beta_2
$$

$$
M33 = I_{mb} + \rho \int_R^{R+L_1} X^2 dx + \rho \int_0^{L_2} Y^2 + (R+L_1)^2 dy
$$

$$K11 = EI \int_{R}^{R+L_1} (\frac{d^2\psi_{a1}}{dx^2})^2 dx + EI \int_{0}^{L_2} (\frac{d^2\psi_{b1}}{dy^2})^2 dy$$

$$K12 = EI \int_{R}^{R+L_1} \frac{d^2\psi_{a1}}{dx^2} \frac{d^2\psi_{a2}}{dx^2} dx + EI \int_{0}^{L_2} \frac{d^2\psi_{b1}}{dy^2} \frac{d^2\psi_{b2}}{dy^2}$$

$$K21 = EI \int_{R}^{R+L_1} \frac{d^2\psi_{a1}}{dx^2} \frac{d^2\psi_{a2}}{dx^2} dx + EI \int_{0}^{L_2} \frac{d^2\psi_{b1}}{dy^2} \frac{d^2\psi_{b2}}{dy^2} dy \qquad (21)$$

$$K22 = EI \int_{R}^{R+L_1} (\frac{d^2\psi_{a2}}{dx^2})^2 dx + EI \int_{0}^{L_2} (\frac{d^2\psi_{b2}}{dy^2})^2 dy$$

$$K13 = K23 = K31 = K32 = K33 = 0$$

$$V_1 = -[\rho\int_{0}^{L_2}\beta_1^2 dy + \rho\int_{R}^{R+L_1}\psi_{a1}^2 dx + \rho\int_{0}^{L_2}\psi_{b1}^2 dy] \; q_1\theta^2 -$$

$$[\rho\int_{0}^{L_2}\beta_1\beta_2 dy + \rho\int_{R}^{R+L_1}\psi_{a1}\psi_{a2} dx + \rho\int_{0}^{L_2}\psi_{b1}\psi_{b2} dy] \; q_2\theta^2 -$$

$$[\rho\int_{0}^{L_2}(R+L_1)\psi_{b1} dy - [\rho\int_{0}^{L_2}\beta_1 Y dy] \; \theta^2 -$$

$$[\rho\int_{0}^{L_2}\beta_2\psi_{b1} dy - \rho\int_{0}^{L_2}\beta_1\psi_{b2} dy] \; \dot{q}_2\theta -$$

$$[\rho\int_{0}^{L_2}\beta_2\psi_{b1} dy] \; q_2\theta +$$

$$[\rho\int_{0}^{L_2}\beta_1\psi_{b1} dy] \; \dot{q}_1\theta$$

$$V_2 = -[\rho\int_{0}^{L_2}\beta_1\beta_2 dy + \rho\int_{R}^{R+L_1}\psi_{a1}\psi_{a2} dx + \rho\int_{0}^{L_2}\psi_{b1}\psi_{b2} dy] \; q_1\theta^2 - \qquad (22)$$

$$[\rho\int_{0}^{L_2}\beta_2^2 dy + \rho\int_{R}^{R+L_1}\psi_{a2}^2 dx + \rho\int_{0}^{L_2}\psi_{b2}^2 dy] \; q_2\theta^2 -$$

$$[\rho\int_{0}^{L_2}\beta_2 Y dy + \rho\int_{0}^{L_2}(R+L_1)\psi_{b2} dy] \; \theta^2 -$$

$$[2\rho\int_{0}^{L_2}\beta_2\psi_{b2} dy] \; \dot{q}_2\theta -$$

$$[\rho\int_{0}^{L_2}\beta_1\psi_{b2} dy + \rho\int_{0}^{L_2}\psi_{b1}\beta_2 dy] \; \dot{q}_1\theta -$$

$$[\rho\int_{0}^{L_2}\beta_1\psi_{b2} dy] \; q_1\theta -$$

$$[\rho\int_{0}^{L_2}\beta_2\psi_{b2} dy] \; q_2\theta$$

43

$$V_3 = [2\rho\int_0^{L_2}\beta_2^2 dy + 2\rho\int_R^{R+L_1}\psi_{a2}^2 dx + 2\rho\int_0^{L_2}\psi_{b2}^2 dy]\ q_2\dot{q}_2\theta\ +$$

$$[2\rho\int_0^{L_2}\beta_1^2 dy + 2\rho\int_R^{R+L_2}\psi_{a1}^2 dx + 2\rho\int_0^{L_2}\psi_{b1}^2 dy]\ q_1\dot{q}_1\theta\ +$$

$$[2\rho\int_0^{L_2}\beta_1\beta_2 dy + 2\rho\int_R^{R+L_1}\psi_{a1}\psi_{a2} dx + 2\rho\int_0^{L_2}\psi_{b1}\psi_{b2} dy]\ q_2\dot{q}_1\theta\ +$$

$$[2\rho\int_0^{L_2}(R+L_1)\psi_{b1} dy + 2\rho\int_0^{L_2}\beta_1 Y dy]\ \dot{q}_1\theta\ +$$

$$[2\rho\int_0^{L_2}(R+L_1)\psi_{b2} dy + \rho\int_0^{L_2}\beta_2 Y dy]\ \dot{q}_2\theta\ +$$

$$[2\rho\int_0^{L_2}\beta_1\beta_2 dy + 2\rho\int_R^{R+L_1}\psi_{a1}\psi_{a2} dx + 2\rho\int_0^{L_2}\psi_{b1}\psi_{b2} dy]\ q_1\dot{q}_2\theta\ +$$

$$[\rho\int_0^{L_2}\beta_1^2 dy + \rho\int_R^{R+L_1}\psi_{a1}^2 dx + \rho\int_0^{L_2}\psi_{b1}^2 dy]\ q_1^2\theta\ +$$ (23)

$$[2\rho\int_0^{L_2}\beta_1\beta_2 dy + 2\rho\int_0^{R+L_1}\psi_{a1}\psi_{a2} dy + 2\rho\int_0^{L_2}\psi_{b1}\psi_{b2} dy]\ q_1 q_2\theta\ +$$

$$[\rho\int_0^{L_2}\beta_2^2 dy + \rho\int_R^{R+L_1}\psi_{a2}^2 dx + \rho\int_0^{L_2}\psi_{b2}^2 dy]\ q_2^2\theta\ +$$

$$[2\rho\int_0^{L_2}(R+L_1)\psi_{b1} dy + 2\rho\int_0^{L_2}\beta_1 Y dy]\ q_1\theta\ +$$

$$[2\rho\int_0^{L_2}(R+L_1)\psi_{b2} dy + 2\rho\int_0^{L_2}\beta_2 Y dy]\ q_2\theta\ - [\rho\int_0^{L_2}\beta_2\psi_{b1} dy]\ \dot{q}_1 q_2\ -$$

$$[\rho\int_0^{L_2}\beta_2\psi_{b1} dy - \rho\int_0^{L_2}\beta_1\psi_{b2} dy]\ \dot{q}_1\dot{q}_2\ - [\rho\int_0^{L_2}\beta_2\psi_{b2} dy]\ \dot{q}_2^2\ -$$

$$[\rho\int_0^{L_2}\beta_2\psi_{b2} dy]\ q_2\ddot{q}_2\ + [\rho\int_0^{L_2}\beta_1\psi_{b1} dy]\ q_1\ddot{q}_1\ -$$

$$[\rho\int_0^{L_2}\beta_1\psi_{b1} dy]\ \dot{q}_1^2\ - [\rho\int_0^{L_2}\psi_{b1}\beta_1 dy]\ q_1\ddot{q}_1$$

44

The spatial variables can be determined in several ways.
The assumed-method (Kane, 1983, pp. 318-319) makes the
approximation that the deflection of each flexible link can
be expressed as a sum of a finite number of spatial mode
shapes that satisfy the given boundary conditions. For a
uniform cantilever free-free or fixed-free beam, the
components of the spatial variables have been calculated by
numerous sources.

The experimental set-up, however, is not a simple
cantilever/free-free continuous beam construction and
therefore would not conform to the above simplification.
Therefore, a finite element analysis of the flexible arm was
conducted to determine the first two mode shapes. The
finite element analysis program GIFTS was used to create a
model of a continuous aluminum bar. Point mass loads were
introduced at the position of the mass intensifiers and the
aluminum connecting elbow and end braces. The structure was
divided into forty nodes.

For a fixed-free representation, the position $X=R_{mainbody}$
was supported in the finite element analysis model. From
the GIFTS analysis, unit deflections for each mode shape
could be determined. Only the first two modes were
analyzed. Each unit was arbitrarily determined to be one
inch. By adding the unit deflection to the original
position, a polynomial could be fitted for each mode shape

(Figures 12 & 13). Therefore, the spatial variables are as follows:

$$\psi_{a1} = -.0057\ X^2 - .0345\ X + .0679$$
$$\psi_{b1} = .0009\ Y^2 + .3233\ Y + 27.72$$
$$\psi_{a2} = -.0025\ X^2 + .2462\ X - .4822 \tag{24}$$
$$\psi_{b2} = .0074\ Y^2 + .1958\ Y + 25.17$$

The vertical deflection of Arm A endpoint can be determined by evaluating this function to be:

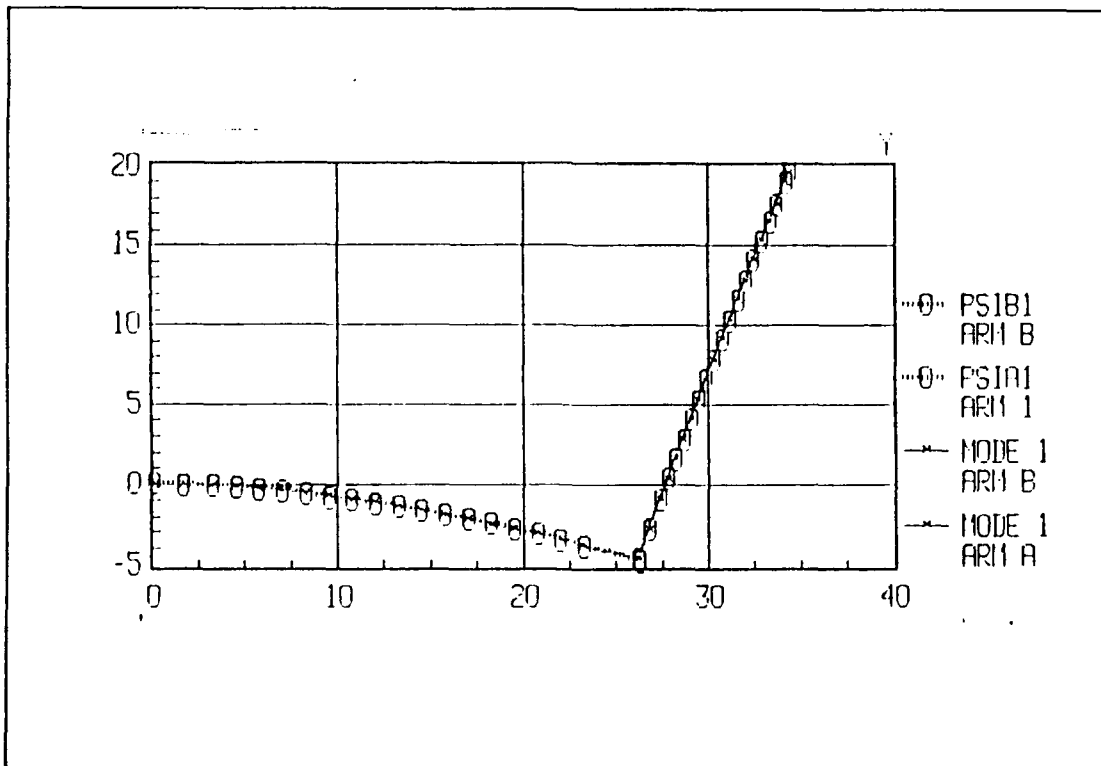$$\beta_1 = -4.77$$

$$\beta_2 - 4.26$$

Figure 12 MODE 1 FINITE ELEMENT ANALYSIS
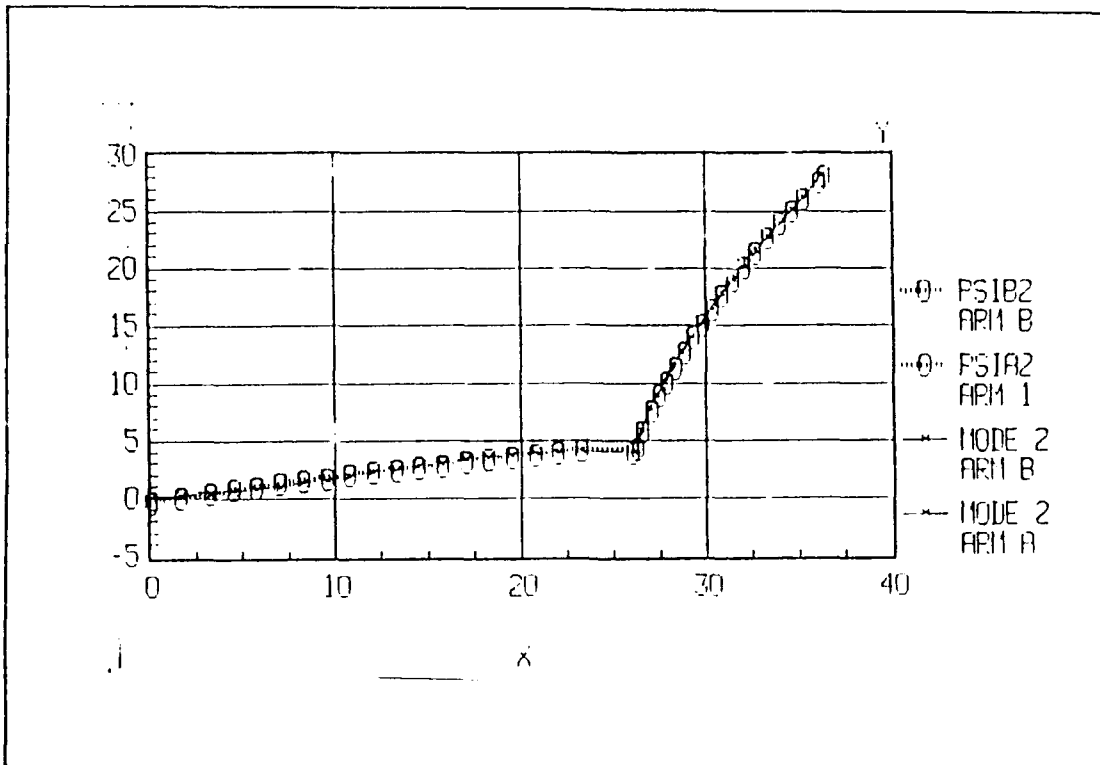VS. POLYNOMIAL FIT.

Figure 13 MODE 2 FINITE ELEMENT ANALYSIS
VS. POLYNOMIAL FIT.

Performing the assigned integration results in the

solution of the matrix variables as follows:

$$
\begin{aligned}
M11 &= 202.84 \\
M12 &= -44.65 \\
M13 &= -316.25 \\
M21 &= -44.65 \\
M22 &= 179.05 \\
M23 &= 170.81 \\
M31 &= -316.25 \\
M32 &= 170.81 \\
M33 &= I_{mb} + 168.14
\end{aligned}
$$

(25)

47

$$V_1 = -153.18 \; q_1\dot{\theta}^2 - 18.57 \; q_2\theta^2 -$$
$$398.68 \; \theta^2 + 39.84 \; \dot{q}_2\theta -$$
$$19.72 \; q_2\dot{\theta} - 22.08 \; \dot{q}_1\theta$$

$$V_2 = -155.78 \; q_1\theta^2 - 52.50 \; q_2\theta^2 -$$
$$363.07 \; \theta^2 - 35.94 \; \dot{q}_2\theta +$$
$$.4 \; \dot{q}_1\theta + 20.12 \; q_1\dot{\theta} -$$
$$17.97 \; q_2\dot{\theta}$$

$$V_3 = 305.00 \; q_2\dot{q}_2\theta + 306.36 \; q_1\dot{q}_1\theta \qquad (26)$$
$$+ 13.50 \; \dot{q}_1q_2\theta + 13.50 \; q_1\dot{q}_2\theta +$$
$$750.32 \; \dot{q}_1\theta + 711.11 \; \dot{q}_2\theta +$$
$$153.18 \; q_1^2\dot{\theta} + 13.50 \; q_1q_2\dot{\theta} +$$
$$152.50 \; q_2^2\dot{\theta} + 793.90 \; q_1\dot{\theta}$$
$$711.11 \; q_2\dot{\theta} - 19.72 \; \ddot{q}_1q_2 -$$
$$39.84 \; \dot{q}_1\dot{q}_2 - 17.97 \; \dot{q}_2^2 -$$
$$17.97 \; q_2\ddot{q}_2 - 22.08 \; q_1\ddot{q}_1 +$$
$$22.08 \; \dot{q}_1^2 + 22.08 q_1\ddot{q}_1$$

$$\begin{aligned}
K11 &= .71 \\
K12 &= .435 \\
K21 &= .435 \\
K22 &= 1.25
\end{aligned} \qquad (27)$$

B. NATURAL FREQUENCY

When placed in motion, the oscillation of a system that takes place will be at the natural frequency ω_n, which is a property of the system. Damping in small amounts will have little effect on the natural frequency and has been neglected in these preliminary calculations. For a single degree of freedom linear system, the natural frequency can be determined from the equations of motion by:

$$\omega_n^2 = \frac{K}{M} \tag{28}$$

where K is the stiffness matrix

M is the mass matrix

For the experimental set-up:

$$E = 10 \times 10^6 \ lbm/in^4$$

$$I = 2.0345 \times 10^{-5} \ in^4$$

$$\mu = .381 \ lbm/in$$

Ignoring the nonlinear terms, solving the equation for ω_n:

$$\omega_1 = .0460 \ Hz$$
$$\omega_2 = .1004 \ Hz \tag{29}$$

V. CONCLUSIONS AND RECOMMENDATIONS

Based on this work, the following conclusions are reached.

A. SYSTEM DESIGN

The experimental set-up for Phase I study of spacecraft control/structural interaction has been designed. All the actuators and sensors have been selected except the end-point displacement sensing of the arm. The mainbody and the flexible arm have been fabricated.

B. THEORETICAL ANALYSIS

The equations of motion for the experimental model have been derived and natural frequencies determined.

C. EXPERIMENTAL ANALYSIS

The natural frequencies of the flexible arm has been determined experimentally and compared with analytical predictions obtained by using the GIFTS finite element analysis program. The experimental and analytical results are in good agreement except the first mode.

D. RECOMMENDATIONS

1. The analytical model of the experimental set-up needs to be improved by full representations of flexible modes, including control laws, and considering nonlinear effects.

2. Future modal analysis should incorporate a filter to reduce the effects of noise. Force windows and exponential windows are available in the data acquisition system for such a purpose.

3. Modal analysis using the VISTA data acquisition package and IDEAS modal analysis software should be completed on the structure once it is connected together and mounted on the granite table on airpads. Natural frequencies and mode shapes should be then determined.

REFERENCES

Agrawal, B., <u>Design of Geosynchronous Spacecraft</u>, Prentice-Hall, Inc., 1986.

Ewins, D. J., <u>Modal Testing; Theory and Practice</u>, Research Studies Press, Ltd., 1984.

Hewlett Packard, <u>The Fundamentals of Modal Testing, Application Note 243-3</u>, Hewlett-Packard Co., 1986.

Juang, K., Yang, L., Huang, J., <u>Rapid Rotational/Translational Maneuvering Experiments of a Flexible Steel Beam</u>, Department of Mechanical Engineering and Mechanics, Old Dominion University, 1989.

Junkins, J. L., <u>Large Angle Maneuvers with Vibration Suppression: Analytical and Experimental Results</u>, Department of Aerospace Engineering, Texas A&M University, 1989.

Kane, T., Likins, P., Levinson, D., <u>Spacecraft Dynamics</u>, McGraw Hill, 1983.

Meirovitch, L., <u>Analytical Methods in Vibrations</u>, The Macmillan Company, 1967.

Meirovitch, L., <u>Dynamics and Control of Structures</u>, John Wiley & Sons, 1990.

Oakley, C.M., Cannon, R.H., <u>Initial Experiments on the Control of a Two-link Manipulator with a Very Flexible Forearm</u>, Department of Mechanical Engineering, Stanford University, 1988.

PCB Piezotronics, Inc., <u>Operating Instructions, Impact Hammer Instrumentation for Structural Behavior Testing</u>, PCB, 1983.

INITIAL DISTRIBUTION LIST

1. Defense Technical Information Center   2
   Cameron Station
   Alexandria, Virginia 22304-6145

2. Library, Code 52   2
   Naval Postgraduate School
   Monterey, California 93943-5000

3. Commander   1
   Naval Space Command
   Attn: Code N152
   Dahlgren, Virginia 22448

4. United States Space Command   1
   Attn: Technical Library
   Peterson AFB, Colorado 80914

5. Director   1
   Navy Space Systems Division (OP-943)
   Washington, DC 20350-2000

6. Space Systems Academic Group, Code SP   1
   Naval Postgraduate School
   Monterey, California 93943-5000

7. Operational Test and Evaluation Force   1
   Modeling and Simulation Branch
   Norfolk, Virginia 23511-5000